Ultrastructure of light-activated axons following optogenetic stimulation to produce late-phase long-term potentiation

Masaaki Kuwajima[1¶], Olga I. Ostrovskaya[1¶], Guan Cao[1], Seth A. Weisberg[2], *Kristen M. Harris[1,2], *Boris V. Zemelman[1,2]

[1]Center for Learning and Memory, The University of Texas at Austin, Austin, Texas, United States of America

[2]Department of Neuroscience, The University of Texas at Austin, Austin, Texas, United States of America

*Corresponding authors

E-mail: kharris@mail.clm.utexas.edu (KMH) and zemelmanb@mail.clm.utexas.edu (BVZ)

¶These authors contributed equally to this work.

Short title: Ultrastructure of optogenetically produced L-LTP

Abstract

Analysis of neuronal compartments has revealed many state-dependent changes in geometry but establishing synapse-specific mechanisms at the nanoscale has proven elusive. We co-expressed channelrhodopsin2-GFP and mAPEX2 in a subset of hippocampal CA3 neurons and used trains of light to induce late-phase long-term potentiation (L-LTP) in area CA1. L-LTP was shown to be specific to the labeled axons by severing CA3 inputs, which prevented back-propagating recruitment of unlabeled axons. Membrane-associated mAPEX2 tolerated microwave-enhanced chemical fixation and drove tyramide signal amplification to deposit Alexa Fluor dyes in the light-activated axons. Subsequent post-embedding immunogold labeling resulted in outstanding ultrastructure and clear distinctions between labeled (activated), and unlabeled axons without obscuring subcellular organelles. The gold-labeled axons in potentiated slices were reconstructed through serial section electron microscopy; presynaptic vesicles and other constituents could be quantified unambiguously. The genetic specification, reliable physiology, and compatibility with established methods for ultrastructural preservation make this an ideal approach to link synapse ultrastructure and function in intact circuits.

Introduction

The cellular correlates of learning and memory have been the subjects of intense study and speculation. We and others have used patterns of activity that produce late-phase long-term potentiation (L-LTP), a form of synaptic plasticity resulting in an increased synaptic efficacy. L-LTP is protein synthesis dependent and lasts more than three hours. Although some structural changes occur early following the induction of LTP, the lasting changes are most likely to reflect mechanisms of memory. *Post hoc* three-dimensional reconstruction from serial section electron microscopy (3DEM) of synapses and resident structures has revealed alterations that occur and are sustained long after the induction of LTP [1–4]. Mechanistic interpretation has been limited, however, because it has only been possible to compare subpopulations of synapses near LTP-producing versus control sites, rather than identify potentiated synapses. Genetic targeting to tag and stimulate individual cells can be achieved by co-expressing channelrhodopsin2 (ChR2) and a modified ascorbate peroxidase [5,6]. Here, we adapted this approach to potentiate a subset of CA3→CA1 hippocampal axons and to identify synapses recently involved in L-LTP.

Optical modulation of plasticity is routinely used across brain areas, and *in vivo* experiments have revealed a correlation between behavioral memory and optically-induced synaptic plasticity (LTP and long-term depression [LTD]) [7,8]. In slice preparations, past efforts using various protocols to induce LTP using ChR2 have been limited to whole-cell recordings and short post-induction times [9–12]. In the hippocampal CA3→CA1 pathway, a previous study used optical stimulation to induce late-phase LTD *in vivo* [13]; however, in this pathway, optically induced L-LTP to our knowledge has not been demonstrated.

We expressed ChR2 and labeled a subset of CA3→CA1 Schaffer collateral and commissural fiber axons using a single virus and then produced L-LTP using high-frequency light pulses. This approach generated a mosaic of labeled and unlabeled axons and allowed a within-preparation comparison of identified synapses having distinct histories of activation. As proof of concept, we reconstructed a labeled axon through 3DEM from a slice that displayed optically induced L-LTP. The tissue quality was superb, demonstrating that we could identify genetically tagged activated axons. The approach proved compatible with conventional tissue fixation and the processing methods needed to preserve subcellular organelles. Hence, it provides a reliable strategy to study synapse-specific mechanisms of synaptic plasticity.

Materials and methods

Animals

This study was carried out in accordance with the recommendations in the Guide for the Care and Use of Laboratory Animals of the National Institutes of Health. All animal procedures were approved by the University of Texas at Austin Animal Care and Use Committee (protocol number AUP-2012-00056 and its successors). All mice were housed under reversed light/dark cycles in an AAALAC-accredited facility managed by the University of Texas Animal Resource Center. We used 8-12 week old male 129S6/SvEvTac mice (Taconic Biosciences, RRID:IMSR_TAC:129sve) for all LTP experiments. Male C57B/6J mice (The Jackson Laboratory, RRID:IMSR_JAX:000664) were also used for earlier experiments, which are indicated as such in figure captions where applicable. All efforts were made to minimize suffering.

AAV assembly and production

A channelrhodopsin2$^{ET/TC}$ [14] fusion protein was assembled with superfolder green fluorescent protein (GFP) [15] fitted with C-terminal Kir2.1 ER export signal [16]. To generate mAPEX2, we modified the wild type ascorbate peroxidase from *P. sativum* (APX) [17] to include an N-terminal palmitoylation tag from growth-associated protein 43 (GAP-43) [18], amino acid substitutions K14D, W41F, E112K [5], and A134P [6], and a C-terminal hemagglutinin epitope tag (HA tag: YPYDVPDYA). ChR2 and codon-optimized mAPEX2 were separated by the self-cleaving porcine teschovirus P2A peptide [19] to produce both proteins from a single transcript. In earlier experiments, we used a version of the rAAV that encoded myc-tagged mAPEX1 with the first three mutations instead of mAPEX2 (indicated in figure captions where applicable).

In addition to the two proteins, the recombinant adeno-associated virus (rAAV) construct comprised an enhanced human synapsin promoter [20], the woodchuck post-transcriptional regulatory element and SV40 polyadenylation sequence. Viruses were assembled using a modified helper-free system (Stratagene) as serotype 2/1 (*rep/cap*) and purified on sequential cesium gradients according to published methods [21]. Titers were measured using a payload-independent qPCR technique [22]. Typical titers were $>10^{10}$ viral genomes/μl.

93 # Rat hippocampal neurons

94 Hippocampal neurons obtained from rats (embryonic day 19) were grown in dissociated cultures [23] on
95 coverslips and were infected on day 8 after plating with the rAAV construct encoding mAPEX1. At 6-10 days
96 post-infection, the neurons used for immunostaining were fixed with 4% formaldehyde in phosphate-buffered
97 saline (PBS) for 15 min. For labeling with 3,3′-diaminobenzidine (DAB; Sigma-Aldrich), the neurons were fixed
98 for 30 min with 2% formaldehyde and 6% glutaraldehyde. All glutaraldehyde-containing fixative was prepared
99 in 0.1 M sodium cacodylate buffer (pH = 7.4) with 2 mM $CaCl_2$ and 4 mM $MgSO_4$.

100 # Stereotaxic injections

101 Mice under isoflurane anesthesia (1-4% mixed in O_2) were placed in a stereotaxic apparatus and
102 prepared for injections with craniotomies over the hippocampal area CA3. Unilateral injections were performed
103 using a pulled glass pipette (10-15 μm diameter tip) mounted on a Nanoject II small-volume injector
104 (Drummond Scientific). Approximately 30 nl of virus was deposited at each injection site at 1-2 minute intervals
105 (from bregma in mm: AP +1.9, ML -2.3, DV 1.8, 1.6, 1.4; AP +2.1, ML -2.5, DV 1.8, 1.6, 1.4). The pipette was
106 left in place for 3–5 min before being removed from the brain. Carprofen (5 mg/kg, sc; TW Medical Cat# PF-
107 8507) was injected 20 min before the end of surgery, and mice were monitored daily thereafter to ensure full
108 recovery. Two rAAV-injected mice (129S6/SvEvTac) were perfusion-fixed under heavy isoflurane anesthesia
109 with 4% paraformaldehyde in 0.02 M phosphate buffer (PB) to verify injection sites, and 15 mice (four
110 129S6/SvEvTac and 11 C57B/6J) were perfusion-fixed with glutaraldehyde (up to 2.5%) and formaldehyde (up
111 to 2%), followed by 20 mM glycine in cacodylate buffer to quench free aldehydes, to verify enzymatic activity of
112 mAPEX2 with Ni-DBA staining as described below.
113

114 # Histology and light microscopy

115 For immunostaining, the fixed neurons were permeabilized with 0.2% Triton X-100 in PBS for 5 min,
116 rinsed in PBS, and blocked in 5% bovine serum albumin (BSA; Sigma-Aldrich) and 5% normal goat serum
117 (NGS; VectorLabs) for 15 min. The cells were then incubated overnight at 4°C with rabbit anti-myc (1:250;
118 Sigma-Aldrich Cat# C3956, RRID:AB_439680) in PBS with 2% BSA, 3% NGS, 0.1% Triton X-100, followed by

119 PBS washes and incubation for 1 hr with goat anti-rabbit IgG conjugated with Cy5 (1:100; Jackson
120 ImmunoResearch Labs Cat# 111-175-144, RRID:AB_2338013) in PBS with 2% BSA, 3% NGS, 0.1% Triton X-
121 100. After PBS washes, the coverslips containing neurons were mounted on glass microscope slides with
122 Aqua/Poly antifade mountant (PolyScience) for epifluorescence microscopy.

123 For DAB-labeling, the neurons were rinsed with cacodylate buffer and treated with 20 mM glycine. Then
124 the neurons were rinsed several times before being incubated with DAB (0.5 mg/ml) and H_2O_2 (0.03%) in
125 cacodylate buffer for 30 min. After buffer rinses, the coverslips were dehydrated in ethanol, cleared in xylenes,
126 and mounted on glass slides with DPX (Electron Microscopy Sciences) for brightfield microscopy.

127 To verify injection sites, the perfusion-fixed brain was vibratome-sectioned (100 μm thickness) for
128 epifluorescent microscopy to visualize GFP. To assess enzymatic activity of mAPEX2, the vibratome-sections
129 (50 μm thickness) of the fixed brain containing the dorsal hippocampus were incubated with Ni-DAB solution
130 (2.5 mM ammonium Ni [II] sulfate and 0.8 mM DAB in 0.1 M PB) for 20 min, before H_2O_2 (final concentration
131 0.0003%) was added and incubated for 10 min. After PB rinses, some of the Ni-DAB labeled sections were
132 processed for EM as described below. Otherwise, they were mounted on glass microscope slides, dehydrated
133 in ethanol, cleared with xylenes, and coverslips were applied with DPX. Epifluorescence and brightfield images
134 were acquired on a Zeiss Axio Imager.Z2 microscope with AxioCamMR3 camera, or a Zeiss Axio Imager.M2
135 with AxioCamHRc3 camera.

136 Instead of the TSA labeling (described below), some of the vibratome sections collected from fixed
137 hippocampal slices were permeabilized and blocked with PBS containing 0.3% Triton X-100, 1% BSA, and
138 10% NGS. The vibraslices were then incubated for overnight at RT with rabbit anti-HA antibody (1:1000; Cell
139 Signaling Technology Cat# 3724, RRID:AB_1549585), followed by 1 hr with the Cy5-conjugated goat anti-
140 rabbit IgG. After PBS rinses, the vibraslices were mounted on glass microscope slides and coverslips were
141 applied with Aqua/Poly mountant for imaging with a Leica TCS SP5 confocal microscope. Single channel
142 stacks (8 bit, 2048 × 2048 pixels at 28.6 nm/pixel) were acquired for GFP (458 nm laser) and Cy5 (633 nm
143 laser) with 63× objective (oil, NA 1.32) at 4× zoom.
144

145 ## Slice preparation, electrophysiology, optical stimulation

146 Six weeks after rAAV injections, the mice were anesthetized deeply with isoflurane and then
147 decapitated. The brain was removed from the cranium, and the left hippocampus was dissected out and rinsed
148 with room temperature (RT) artificial cerebrospinal fluid (aCSF; pH = 7.4) containing (in mM) 117 NaCl, 5.3
149 KCl, 26 $NaHCO_3$, 1 NaH_2PO_4, 2.5 $CaCl_2$, 1.3 $MgSO_4$, and 10 D-glucose, and bubbled with 95% O_2-5% CO_2.
150 Slices (400 μm thickness; 4 per animal) from the dorsal hippocampus were cut at 70° transverse to the long
151 axis on a Stoelting tissue chopper and transferred in oxygenated aCSF to the supporting nets of interface
152 chambers in the Synchroslice system (Lohmann Research Equipment). The entire dissection and slice
153 preparation took ~5 min. This rapid dissection, together with the interface chamber design, provides for high-
154 quality ultrastructure during long acute slice experiments [24–27]. Hippocampal slices were placed on a net at
155 the liquid-gas interface between 30-31°C aCSF and humidified 95% O_2-5% CO_2 atmosphere bubbled through
156 35-36°C deionized water. For experiments in which the area CA3 was cut, the dissection was made using the
157 25-gauge needle on a 1-ml syringe after the slices were transferred into the chambers.

158 After 3 hr of incubation, the optical fiber (300 μm core diameter; 0.39 NA; ThorLabs FT300UMT) and
159 recording electrode (Thomas Recording) were positioned 400-600 μm apart in middle *stratum radiatum* of the
160 area CA1 with the fiber placed toward the area CA3. An optimal position of the recording electrode was chosen
161 by probing several points across CA1 and SR to achieve larger responses. One-ms pulses of laser (λ = 473
162 nm; maximal output ~14.5 mW as measured by a Thorlabs S130C light meter) were delivered from source
163 (ThorLabs S1FC473MM) controlled by a pulse generator (A.M.P. Instruments Master-8). The light meter
164 placed directly under the hippocampal slices showed approximately 30% loss of laser power through the slice
165 thickness, while the recording site was approximately 100 μm deep from the top surface. GluN receptors were
166 blocked by adding 4 μl of 25 mM d,l-2-amino-5-phosphonovaleric acid (APV; Abcam Cat# ab144498) to the 1
167 ml of aCSF in the interface recording chamber, which achieved an effective concentration of 50 μM d-APV.
168 Tetrodotoxin (TTX; final concentration 1 μM; Abcam Cat# ab120055) and 6,7-dinitroquinoxaline-2,3-dione
169 (DNQX; final concentration 20 μM; Abcam Cat# ab144496) were added to block voltage-gated sodium
170 channels and GluA receptors, respectively.

171 For electrical stimulation experiments, we replaced the optical fiber with a concentric bipolar electrode
172 (FHC, Inc.), which was used to deliver 200 μs biphasic current pulses (100-300 μA), lasting 100 μs each for
173 positive and negative components of the stimulus. The initial eEPSP slope was ~50% of the maximal eEPSP
174 slope based on the input-output (IO) curve for each slice. IO curves were recorded by using a sequence of
175 pulses applied each 30 s with increasing stimulus intensity in 25 μA increments. Test pulses were given at 1
176 pulse per 2.5 min unless stated otherwise, and eEPSP was recorded. Paired-pulse ratio (PPR) was measured
177 by applying two optical stimuli spaced 50-200 ms apart with 50 ms increment, every 30 s.
178

179 Microwave-enhanced chemical fixation of hippocampal slices and TSA 180 labeling

181 At end of recordings, the slices were immersed in fixative containing 1% glutaraldehyde and 4%
182 formaldehyde, and were microwaved immediately for 8-10 s at 700 W (modified from ref. 27). The fixed slices
183 were stored overnight at RT in the same fixative or in cacodylate buffer. After being immersed in 20 mM
184 glycine for 20 min and buffer rinses, the area CA1 was dissected out under a stereoscope with a microknife
185 and embedded into 9% agarose. Vibratome sections (50 μm thickness) were then collected from the area of
186 optical stimulation to the location of the recording electrode. ChR2-GFP expression was confirmed with
187 epifluorescence microscopy. The sections were transferred to 0.1 M PB and then incubated with tyramide-
188 conjugated Alexa Fluor 647 (Thermo Fisher Scientific Cat# T20951) for 15 min in dark before H_2O_2 was added
189 (final concentration 0.0015%) and incubated for additional 10 min in dark. After washes with PB, the vibraslices
190 were washed in cacodylate buffer before being processed for 3DEM.
191

192 Tissue processing for 3DEM

193 TSA-labeled vibratome section was embedded into 9% agarose to protect it during the subsequent
194 processing, as described previously [28,29]. The tissue was immersed for 5 min in reduced osmium solution
195 containing 1% osmium tetroxide (OsO_4; Electron Microscopy Sciences) and 1.5% potassium ferrocyanide
196 (Sigma-Aldrich) in cacodylate buffer. After several buffer rinses, the tissue was immersed in 1% OsO_4 and two

197 cycles of microwave irradiation (175 W; 1 min on → 1 min off → 1 min on) were applied with cooling to ~15°C
198 in between. The tissue was rinsed in buffer several times, twice in purified water, and then immersed in 50%
199 ethanol before being dehydrated in ascending concentrations of ethanol (50%, 70%, 90%, 100%) containing
200 1% uranyl acetate (UA; Electron Microscopy Sciences) with application of microwave irradiation (250 W, 40 s
201 per ethanolic UA step). Ethanol was replaced by propylene oxide, and the tissue was infiltrated and embedded
202 into LX-112 resin (Ladd Research). Embedded tissue was trimmed under a stereomicroscope to expose the
203 region of interest containing the middle *stratum radiatum* of the area CA1. Serial thin sections (~60 nm
204 thickness) were cut with a diamond knife (Diatome Ultra35) on a ultramicrotome (Leica Ultracut UC6 or UC7)
205 and collected on Synaptek TEM grids (Be-Cu or gilded; Electron Microscopy Sciences or Ted Pella) coated
206 with film of polyetherimide (PEI; Goodfellow).
207

208 Post-embedding immunogold labeling and gold enhancement

209 Serial thin sections on gilded grids (4-6 sections per grid) were rinsed with Tris-buffered saline (TBS;
210 pH = 7.6) containing 0.01% Triton X-100 (TBS-T) and then blocked with 2% human serum albumin (HSA;
211 Sigma-Aldrich) and 10% NGS in TBS-T for 30 min. The sections were then incubated overnight at 4°C with
212 TBS-T containing 1% HSA, 1% NGS, and mouse anti-Cy5/Alexa Fluor 647 (cocktail of antibodies at 1:100
213 each from Sigma-Aldrich [Cat# C1117, RRID:AB_477654] and Miltenyi Biotec [custom-ordered antibody used
214 in their Anti-Cy5/Anti-Alexa Fluor 647 MicroBeads, Cat# 130-091-395]). After extensive washes with TBS-T
215 and TBS (pH = 8.2; TBS-8.2), the sections were incubated for 90 min at RT with TBS-8.2 containing 1% NGS,
216 0.5% polyethylene glycol, and goat anti-mouse antibody conjugated with colloidal gold (5 or 15 nm diameter;
217 BBI Solutions Cat# EM.GMHL5 or EM.GMHL15; 1:100). The sections were subsequently washed with TBS-8.2
218 containing additional 500 mM NaCl to reduce nonspecific antibody binding and then with TBS-8.2. The
219 sections labeled with 5 nm gold were further rinsed with purified water, incubated with gold enhancement
220 solution (GoldEnhance EM Plus; Nanoprobes) for 5 min at RT under ambient room light, and extensively
221 washed in purified water. Shortening the incubation time for gold enhancement should reduce formation of
222 background particles. All sections were stained with saturated aqueous solution of UA followed by lead citrate
223 [30] for 5 min each.

Acquisition, alignment, and analysis of serial tSEM images

Serial section images (8-bit TIFF; field size = 24,576 × 24,576 pixels) were acquired on a Zeiss Supra40 field emission scanning electron microscope in transmission mode (tSEM) [31] with ATLAS package, running at 28 kV, at 1.8 nm pixel size with 1.2 μs dwell time and 3.5 mm working distance. Serial tSEM images were aligned automatically using Fiji [32] (RRID:SCR_002285; http://fiji.sc) with the TrakEM2 plugin [33] (RRID:SCR_008954; http://www.ini.uzh.ch/~acardona/trakem2.html). The images were aligned rigidly first, followed by application of elastic alignment [34]. The aligned image stack was cropped to 14,424 × 19,512 pixels with Fiji/TrakEM2 and imported into Reconstruct [35] (RRID:SCR_002716; http://synapseweb.clm.utexas.edu/software-0) for 3D reconstruction and analyses. An image of grating replica (Electron Microscopy Sciences Cat# 80051), acquired along with serial section images, was used to calibrate pixel size. Mean section thickness was estimated based on the diameter of longitudinally sectioned mitochondria [36]. In serial tSEM images of sections that were immunolabeled, we first identified all axons containing any gold particles. An axon was considered as positively labeled if it contained gold particles (> 10 nm diameter after gold enhancement) outside mitochondria in at least two of three serial sections. To measure the density of enhanced gold particles, all particles were counted in four immunolabeled sections and categorized as positive labels or background. Particle densities were calculated from these counts divided by their respective areas in each of the analyzed sections.

Control for immunogold labeling

To control for non-specific labeling by the secondary antibody, some serial thin sections underwent immunogold labeling with the primary antibody omitted. These sections showed minimal background gold labels that were distributed throughout the tissue surface. To control for self-nucleation of gold enhancement reagent, a tSEM image was also acquired from serial thin sections of the area CA1 that were not immunolabeled, but were incubated with the gold enhancement reagent as above and then stained with UA and lead citrate.

To measure the size of enhanced gold particles, the antibody conjugated with 5 nm gold was blotted on a PEI-coated TEM grid and then treated with the gold enhancement reagent as above. We acquired a tSEM image from a square field encompassing 4,096 pixels per side at 1.8 nm/pixel and thresholded the image to identify a total of 527 particles for their size measurement with the particle analysis function of Fiji. This measures the maximum caliper, which is the longest distance between any two points along the selection boundary. Enhanced particles that obviously formed from two or more 5 nm particles placed in close proximity, as evidenced by the presence of negative curvatures, were excluded from this analysis.

Confocal image analysis

Fiji was used for processing and analysis of the confocal images. Maximum intensity projection images were generated from 5 optical sections encompassing 51.5 × 34.3 × 3.2 μm in x, y, and z. Image stacks from Cy5 channel were corrected for bleaching (the simple ratio method under bleach correction function in Fiji) before they were projected. Projected images from GFP and Cy5 channels were merged and thresholded to identify all puncta (≥ 100 nm) labeled with either of the fluorophores, which were then assessed for co-expression in single channel images. A total of 682 labeled puncta were identified, excluding those at edges of the image. Acquisition of single channel image stacks for each of the fluorophores, rather than dual-channel stacks, caused a slight mismatch in their z-positions, which may have contributed to a small fraction of puncta to appear as single-labeled.

Analysis of physiology recordings

The initial acquisition and analysis of EPSP were performed with SynchroBrain software (Lohmann Research Equipment). The initial maximum slope was measured over a 0.2-0.8 ms time frame that was held constant for all recordings in each slice. To calculate the magnitude of LTP, EPSP slopes were normalized to the average slopes obtained during the last 30 min of baseline recordings before the delivery of the first HFS. Then values across slices (mean ± SEM) were presented as times baseline. LTP magnitude at 30, 60, 120, and 180 min post-HFS was calculated by averaging the values for the preceding 20 min. Prism software package (Graphpad Software) was used for statistical analysis and plotting. The main tests performed were

Student's t-test and analysis of variance (ANOVA). Specific statistical tests and results are shown in the corresponding figure captions.

Data availability

The following files generated and analyzed during the current study are deposited at Texas Data Repository (doi:10.18738/T8/QP43LB):

1. The original, unaligned serial tSEM images (VYLNH_raw1.zip [11.1 GB], VYLNH_raw2.zip [11.4 GB], and VYLNH_raw3.zip [12.0 GB])
2. The aligned 3DEM dataset (VYLNH_20181017.zip; 14.8 GB)
3. S1 Video (S1_video.mp4; 71.1 MB).

Results

Potentiation of synapses using light

We designed an adeno-associated virus vector (rAAV) for stimulating and tracking individual neurons and the trajectories of their axons. The construct encoded two proteins: a ChR2 [14] fused to GFP [15] and an APX from *P. sativum* [17] to generate the electron-dense deposits detected in EM. We chose $ChR2^{ET/TC}$ based on its conductance and ability to sustain optical stimulation up to 60 Hz [14]. We modified APX to include amino acid substitutions for increased stability and enzymatic activity [5,6]. We enhanced its membrane and synapse targeting by adding a palmitoylation signal from growth-associated protein 43 (GAP-43) [18] to produce mAPEX2 (Fig 1A). A virus encoding ChR2 and mAPEX2 ensured that both proteins co-localized in the same cells. The observations from dissociated neurons and acute hippocampal slices reflect ChR2-GFP and mAPEX2 co-expression at the cellular and synaptic levels (Figs 1B and 1C).

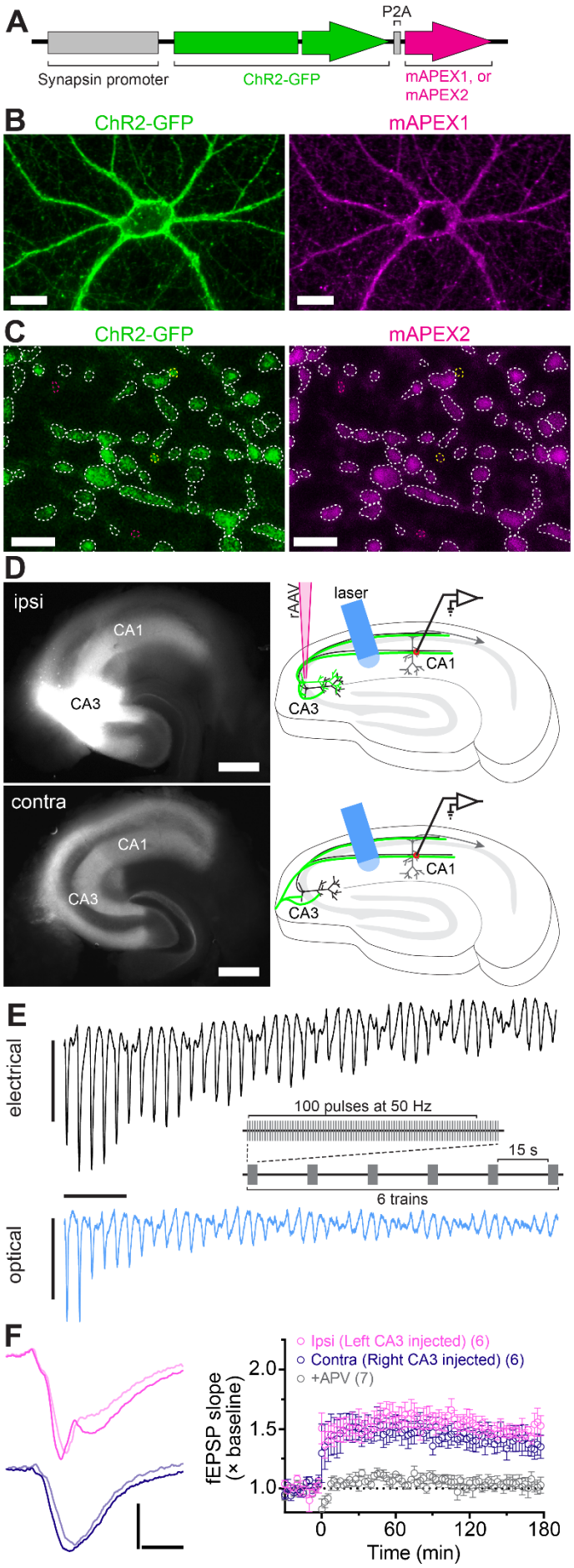
A
P2A
Synapsin promoter
ChR2-GFP
mAPEX1, or
mAPEX2
B
ChR2-GFP
mAPEX1
C
ChR2-GFP
mAPEX2
D
ipsi
CA1
CA3
rAAV
laser
CA1
CA3
contra
CA1
CA3
CA1
CA3
E
electrical
100 pulses at 50 Hz
15 s
6 trains
optical
F
Ipsi (Left CA3 injected) (6)
Contra (Right CA3 injected) (6)
+APV (7)
fEPSP slope
(× baseline)
2.0
1.5
1.0
0
60
120
180
Time (min)

302 **Fig 1. Viral expression of ChR2-GFP and mAPEX, and induction of optical L-LTP.** (**A**) The rAAV was
303 designed to co-express ChR2-GFP and mAPEX under a single synapsin promoter in neurons. During
304 translation, the P2A peptide self-cleaves to yield the two proteins. (**B**) Cultured hippocampal neurons infected
305 with the rAAV co-expressed ChR2-GFP and mAPEX1. Scale bars = 25 μm. (**C**) ChR2-GFP was co-expressed
306 with mAPEX2 in the same axons in the area CA1 (dotted white lines). Yellow and magenta lines indicate
307 ChR2-GFP only and mAPEX2 only puncta, respectively. Scale bars = 2 μm. (**D**) GFP fluorescence images
308 (left) and experimental configurations (right) in ipsilateral (top, ipsi) and contralateral (bottom, contra)
309 hippocampal slices. Scale bars = 500 μm. (**E**) Electrical (top) and optical (bottom) EPSPs evoked by a train of
310 50 Hz stimulations, recorded from CA1 middle *stratum radiatum* (C57B/6J strain). Responses to the first 40
311 pulses are shown and the stimulation artifacts are clipped from the eEPSP data. The inset shows HFS protocol
312 for LTP induction. Scale bars = 1 ms, 2 mV (electrical), 1 mV (optical). (**F**) Optical HFS induced L-LTP in the
313 Schaffer collateral and commissural pathways. *Left:* Representative oEPSP traces from ipsilateral (top) and
314 contralateral (bottom) slices before (light shaded line) and 3 hr after (solid line) HFS. *Right:* Time course of
315 oEPSP slope (mean ± SEM) showing optical L-LTP in ipsilateral (pink) and contralateral (purple) slices.
316 Addition of APV blocked L-LTP (grey). The number of slices is indicated in parentheses. Scale bars = 4 ms, 1
317 mV.
318
319
320 We injected the rAAV vector into *stratum pyramidale* of the hippocampal area CA3 in one hemisphere
321 of the adult mouse brain (S1 Fig, A). Epifluorescence microscopy confirmed robust expression of ChR2-GFP in
322 the CA3 neurons and in Schaffer collaterals extending into ipsilateral area CA1. The contralateral hippocampus
323 showed GFP-labeled commissural/associational fibers in the areas CA1 and CA3 (S1 Fig, B).
324 Four to six weeks after virus injection we prepared acute transverse slices from ipsilateral or
325 contralateral hippocampus, four per hemisphere, covering the dorsal region. The slices were allowed to
326 recover for 3 hr in interface chambers [37]. We then applied pulses of blue light (473 nm wavelength; ~14.5
327 mW power) via an optical fiber (300 μm diameter) positioned over the area CA1 *stratum radiatum* in each
328 chamber (Fig 1D) and examined the ChR2 responses. Typically, 2-4 slices displayed optical responses. In

329 these slices, optically-evoked field excitatory postsynaptic potentials (oEPSP) and population spike shapes
330 recorded within different strata of area CA1 resembled the waveforms observed previously with electrical
331 stimulation (eEPSP) [38–40], confirming a similar propagation of the signal. Although oEPSP were similar to
332 eEPSP, we noticed a difference in the shape of the waveform: the initial activation stage consisted of more
333 than one component, visible as change in slope. We assume this could be due to asynchrony of fiber firing at
334 different sites along *stratum radiatum* because of the relatively larger area stimulated by light compared to
335 concentric bipolar stimulating electrodes. In accordance with prior reports, oEPSP had comparable slopes and
336 amplitudes between ipsilateral and contralateral groups of fibers [11,41], although these parameters were
337 significantly smaller than in electrical responses (S1 Fig, D). Light-evoked short-term plasticity [42], measured
338 as paired-pulse ratio (PPR), was also detected (S1 Fig, E). Optical responses were blocked by TTX (S1 Fig, F)
339 and DNQX (S1 Fig, F), demonstrating their dependence on voltage-gated sodium channels and GluA
340 receptors, respectively.

341 Next, we confirmed that ChR2 could follow trains of light pulses needed to induce L-LTP. Stimuli were
342 delivered at 50 Hz (Fig 1E), a frequency sufficient for LTP induction [10,43] that also allows more time for
343 ChR2 to recover between stimulation episodes [14] than the higher frequencies (100 Hz or higher, including
344 theta-burst) typically used for electrical induction of LTP. Optical stimulation resulted in the trains of evoked
345 oEPSP in CA1 *stratum radiatum* (Fig 1E, bottom) in a pattern comparable to the one evoked by 50 Hz
346 electrical stimulation (Fig 1E, top). However, optical responses exhibited smaller initial amplitudes and
347 underwent stronger desensitization during the trains of light stimuli.

348 Smaller amplitudes in our optical experiments could be due to incomplete ChR2 activation or to the
349 presence of ChR2 in a relatively small subset of axons. To differentiate between these possibilities, we
350 recorded oEPSP under varied light stimulus intensity. Input-output curves of oEPSP slope as a function of light
351 intensity showed an apparent saturation at maximum level of ~14.5 mW (S2 Fig). Thus, our optical stimulation
352 protocol maximized activation of all the targeted axons.

353 Optical stimulus regimes produced L-LTP that lasted for at least 3 hr (Fig 1F). Optically stimulated
354 ipsilateral and contralateral slices showed the same degree of potentiation. However, the likelihood of
355 achieving L-LTP varied, and the success rate was 67% and 42% for ipsilateral and contralateral slices,

356 respectively. Optical L-LTP induction was blocked by application of 2-amino-5-phosphonovaleric acid (APV),
357 reflecting a dependence on GluN receptors (Fig 1F).

358 To isolate the rAAV-targeted CA3 axons as the sole source of excitatory synaptic transmission and to
359 avoid possible recruitment of unlabeled fibers, we recorded oEPSP from contralateral slices with the area CA3
360 severed pre-recovery (Fig 2A). Using contralateral slices additionally eliminated the likelihood that CA1
361 neurons could be labeled with ChR2 and stimulated independently of the CA3 axons. Severing CA3 had little
362 effect on the likelihood or magnitude of L-LTP from electrical stimulation (Fig 2B). In contrast, the induction rate
363 was reduced from 42% to 33% in contralateral sections with severed CA3, and the magnitude of LTP was
364 smaller at 1 hr compared to intact sections, but nearly identical by 3 hr (Figs 2C and 2D). The magnitude of
365 electrical LTP in intact and cut slices was similar at 1 hr and 3 hr post-stimulation (Figs 2B and 2D). We
366 conclude that the optical stimulation of genetically specified CA3 commissural fibers is sufficient to induce L-
367 LTP in the area CA1.

368

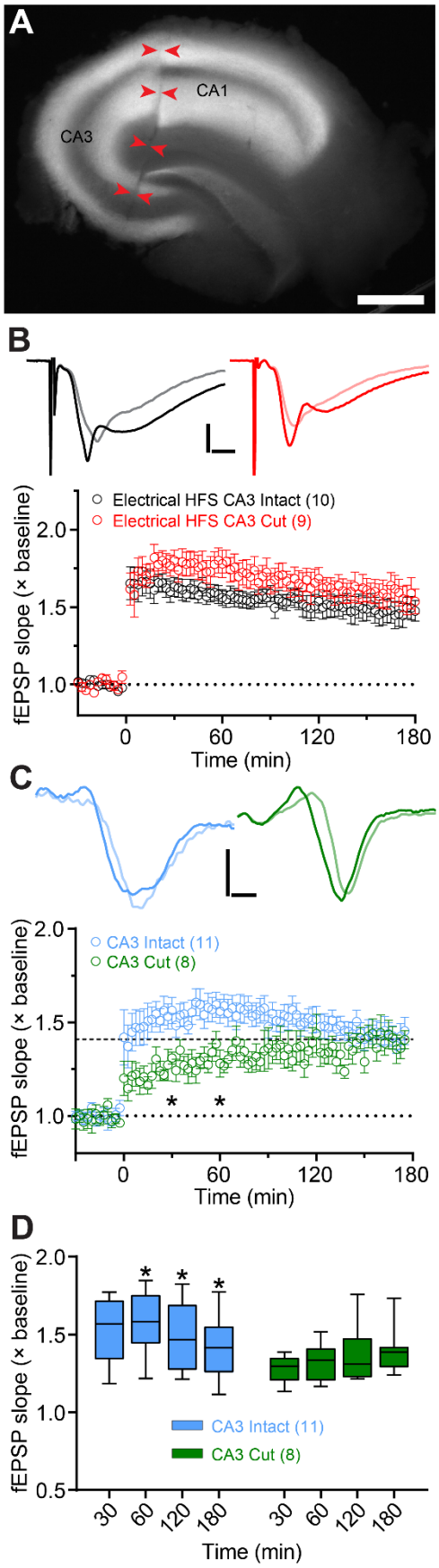
A
CA1
CA3
B
Electrical HFS CA3 Intact (10)
Electrical HFS CA3 Cut (9)
fEPSP slope (× baseline)
2.0
1.5
1.0
0
60
120
180
Time (min)
C
CA3 Intact (11)
CA3 Cut (8)
fEPSP slope (× baseline)
2.0
1.5
1.0
*
*
0
60
120
180
Time (min)
D
fEPSP slope (× baseline)
2.0
1.5
1.0
0.5
*
*
*
CA3 Intact (11)
CA3 Cut (8)
30
60
120
180
30
60
120
180
Time (min)

370 **Fig 2. Optical stimulation of CA3→CA1 commissural fibers was sufficient for L-LTP.** (**A**) Representative
371 image of a contralateral slice with CA3 cut off from CA1. Scale bar = 500 μm. (**B**-**C**). LTP induced by electrical
372 (**B**) and optical (**C**) HFS in intact and cut slices. The example traces show EPSPs recorded before (light
373 shaded lines) and 3 hr after HFS (solid lines). Optical LTP magnitude (**C**) at 30 and 60 min post-HFS was
374 significantly different between intact and cut slices (oEPSP slope $F_{(1, 17)} = 4.74$, $p < 0.05$; Time $F_{(3, 51)} = 0.95$, p
375 > 0.05; Interaction $F_{(3, 51)} = 6.60$, $p < 0.0001$; repeated measures two-way ANOVA with Bonferroni's post-hoc
376 tests). Scale bars = 2 ms, 2 mV (**B**); 1 ms, 0.5 mV (**C**). (**D**) Summary data for oEPSP slope change at different
377 time points following optical HFS in intact and cut slices. The intact slices showed significant changes in LTP
378 magnitude in the last 120 min of recordings ($F_{(1.28, 12.8)} = 5.75$, $p < 0.05$; repeated measures one-way ANOVA).
379 The box plots show medians and interquartile ranges, with whiskers extending from minimum to maximum
380 values. The number of slices used for each condition is indicated in parentheses.
381

382 *Post hoc* labeling and reconstruction of potentiated synapses

383 Post hoc 3DEM analysis of activated synapses and subcellular organelles requires well-preserved slice
384 tissue, which is typically achieved by chemical fixation with glutaraldehyde. Thus, the expressed EM tag must
385 retain its enzymatic activity to produce electron-dense deposits in fixed samples. Like the original APEX [5,6],
386 we verified that mAPEX2 was active after glutaraldehyde fixation by observing conversion of 3,3'-
387 diaminobenzidine (DAB) into osmiophilic polymers, which appear dark brown under light microscopy or as
388 amorphous electron-dense deposits under EM (S3 Fig).
389 We fixed brain slices that displayed L-LTP following optical stimulation at the 3 hr time point and had
390 robust GFP labeling (Fig 3A, Step 1; see Materials and Methods). Orthogonal vibratome sections spanning
391 area CA1 (Fig 3A, Steps 2-3) were incubated with tyramide conjugated with Alexa Fluor 647. Membrane-
392 associated mAPEX2 then catalyzed the tyramide signal amplification reaction (TSA) locally upon the addition
393 of H_2O_2 (Fig 3A, Step 4). After heavy metal staining and epoxy embedding, serial thin sections (~60 nm
394 thickness) were collected from a region of interest containing the middle of *stratum radiatum* (Fig 3A, Steps 5-
395 7). For the series shown in Figs 3A (Step 7), 3C, and 4, a total of 72 sections were collected from portions of
396 tissue at least 10 μm from the surface of a 50 μm thick vibratome section.

397

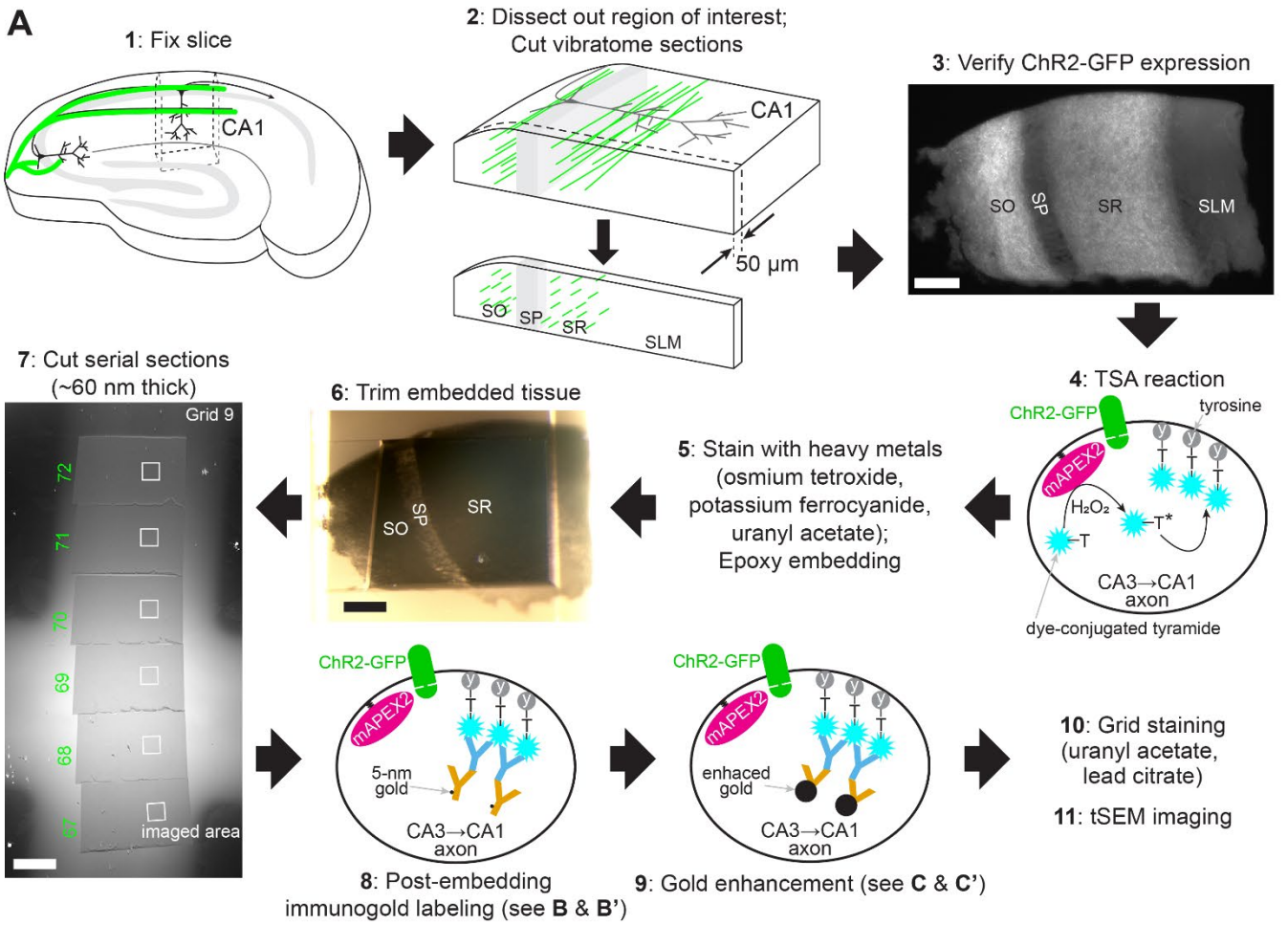
A
1: Fix slice
CA1
2: Dissect out region of interest;
Cut vibratome sections
CA1
50 µm
SO
SP
SR
SLM
3: Verify ChR2-GFP expression
SO
SP
SR
SLM
4: TSA reaction
ChR2-GFP
tyrosine
mAPEX2
H₂O₂
T*
T
CA3→CA1
axon
dye-conjugated tyramide
5: Stain with heavy metals
(osmium tetroxide,
potassium ferrocyanide,
uranyl acetate);
Epoxy embedding
6: Trim embedded tissue
SO
SP
SR
7: Cut serial sections
(~60 nm thick)
Grid 9
72
71
70
69
68
67
imaged area
ChR2-GFP
mAPEX2
5-nm
gold
CA3→CA1
axon
8: Post-embedding
immunogold labeling (see B & B')
ChR2-GFP
mAPEX2
enhaced
gold
CA3→CA1
axon
9: Gold enhancement (see C & C')
10: Grid staining
(uranyl acetate,
lead citrate)
11: tSEM imaging

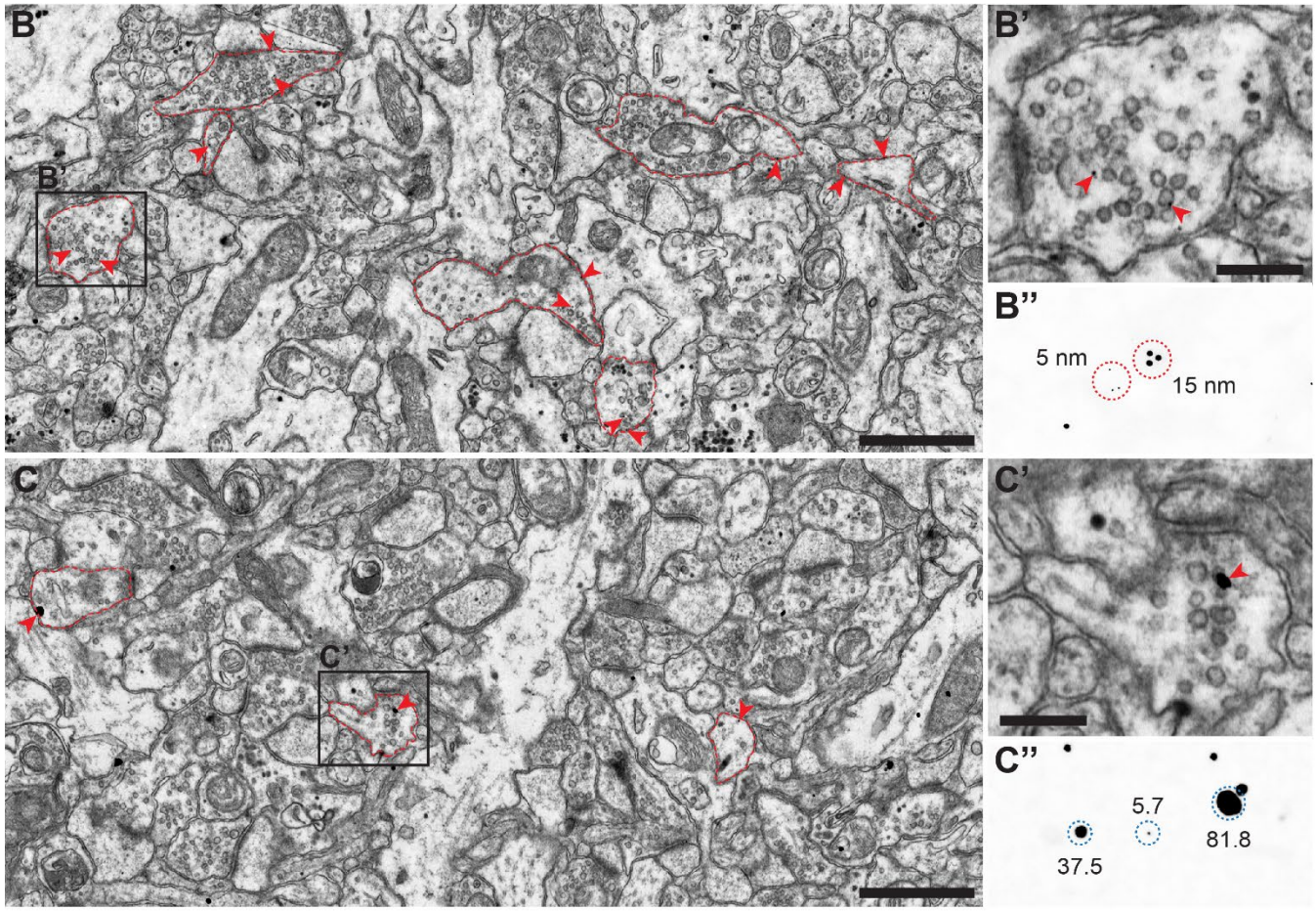
B
B'
B'
B''
5 nm
15 nm
C
C'
C'
C''
5.7
37.5
81.8

399 **Fig 3**. **mAPEX2-catalyzed labeling and 3DEM identification of rAAV-targeted axons.** (**A**) Workflow for
400 processing of hippocampal slices following optical L-LTP. Vibratome sections from the fixed area CA1
401 underwent tyramide signal amplification (TSA) catalyzed by mAPEX2 to deposit Alexa Fluor dye in the targeted
402 axons. The dye-labeled section was then stained with heavy metals and embedded into epoxy before being cut
403 into serial thin sections. The dye-containing axons in a subset of the sections were immunolabeled with 5 nm
404 gold particles, followed by gold enhancement. Scale bars = 100 μm. (**B** and **B'**) A low magnification tSEM
405 image of the area CA1 *stratum radiatum* after immunolabeling (Step 8 in **A**). Axonal boutons indicated by red
406 contours were positively labeled with 5 nm gold particles (red arrowheads). Area indicated by black rectangle is
407 enlarged in **B'**. Scale bar = 1 μm in **B**, 250 nm in **B'**. (**B''**) A tSEM image of colloidal gold particles (5 nm and
408 15 nm). To visualize the 5 nm particles more clearly, this image was acquired at 1 nm/pixel and scaled to the
409 same magnification as **B'**. (**C** and **C'**) Same as **B** and **B'**, imaged after gold enhancement (Step 9 in **A**). Scale
410 bar = 1 μm in **C**, 250 nm in **C'**. (**C''**) A tSEM image of enhanced gold particles. The numbers indicate diameters
411 in nm (also see S5 Fig 5).
412
413 In a subset of sections, at the beginning and end of the series, we labeled the axons expressing
414 mAPEX2 that now contained the dye-tyramide molecules with anti-dye antibodies, then gold-conjugated
415 secondary antibodies (Fig 3A, Step 8). This limited labeling ensured that the ultrastructure was visible while
416 having sufficient labeling to identify the genetically-targeted axons unambiguously (Figs 3B and 3B'). We
417 considered an axon to be positively labeled if it contained gold particles in at least two of three serial sections
418 per grid. We tested 5 nm and 15 nm colloidal gold particles. Staining with smaller particles suffered from
419 relatively low signal-to-noise, limited visibility of the gold particles (nominal particle size = 5 nm vs. pixel size =
420 1.8-2.0 nm), and difficulty in distinguishing the particles from artifacts and subcellular features of similar size
421 (Fig 3B' and S4 Fig). Working with 15 nm gold particles improved particle visibility (Fig 3B'') but reduced
422 labeling sensitivity, making labeled axons harder to identify. We boosted the visibility of 5 nm particles by
423 increasing their size with a gold enhancement technique [44] (Fig 3A, Step 9). The enhanced particles were of
424 high contrast and uniformly electron-dense with smooth edges, which made them distinct from artifacts and
425 subcellular structures of similar size (e.g., glycogen granules, darkly stained membrane, and precipitation from

426 post-section staining; Figs 3C, 3C', and S4 Fig). Enhancement of immunogold particles blotted on a blank grid
427 resulted in particles with diameter ranging from 2.5 nm to 85.3 nm (median = 37.1 nm), significantly improving
428 their ease of identification (Fig 3C'' and S5 Fig). Control sections devoid of immunogold labeling, but treated
429 with the enhancement reagent, showed electron-dense particles with the diameter ≤ 10 nm, likely resulting
430 from reagent self-nucleation (S5 Fig). We therefore excluded these small particles during identification of
431 labeled axons. Thus, in the gold enhanced material, our criterion for positively labeled axons was the presence
432 of particles > 10 nm in diameter in at least two of three consecutive sections. The density of positive particles
433 within labeled axons after gold enhancement was 2.85 ± 0.88 per μm^2, while the overall background particle
434 density was 0.33 ± 0.02 per μm^2 (mean ± SEM; n = 4 sections). Thus, the signal-to noise ratio was 8.7.
435 Finally, we reconstructed a labeled axon from an rAAV-infected CA3 neuron forming synapses onto
436 dendritic spines in middle *stratum radiatum* of the area CA1 from a slice that showed optically induced L-LTP
437 (Fig 4 and S1 Video). This axon contained gold particles in the first three sections and three of the last four
438 sections that were immunolabeled (Figs 4A and 4C). This axon had two multi-synaptic boutons, one of which
439 was reconstructed only partially because it was at one edge of the serial section series (Fig 4B). This partial
440 bouton formed synapses with two spines (s1 and s2 in Fig 4B; also see S1 Video). One of these spines (s1)
441 had another branch that formed a synapse with a separate axonal bouton that was unlabeled. The synapses
442 on the branched spine (s1) were both macular and of similar sizes (0.029 μm^2 and 0.021 μm^2). The bouton that
443 was completely reconstructed contained two mitochondria and formed synapses with two spines from different
444 dendrites (Fig 4B; S1 Video). One of these synapses was perforated (area = 0.11 μm^2), while the other was
445 macular (area = 0.037 μm^2). These findings are consistent with synapses on this axon having been potentiated
446 [45].
447

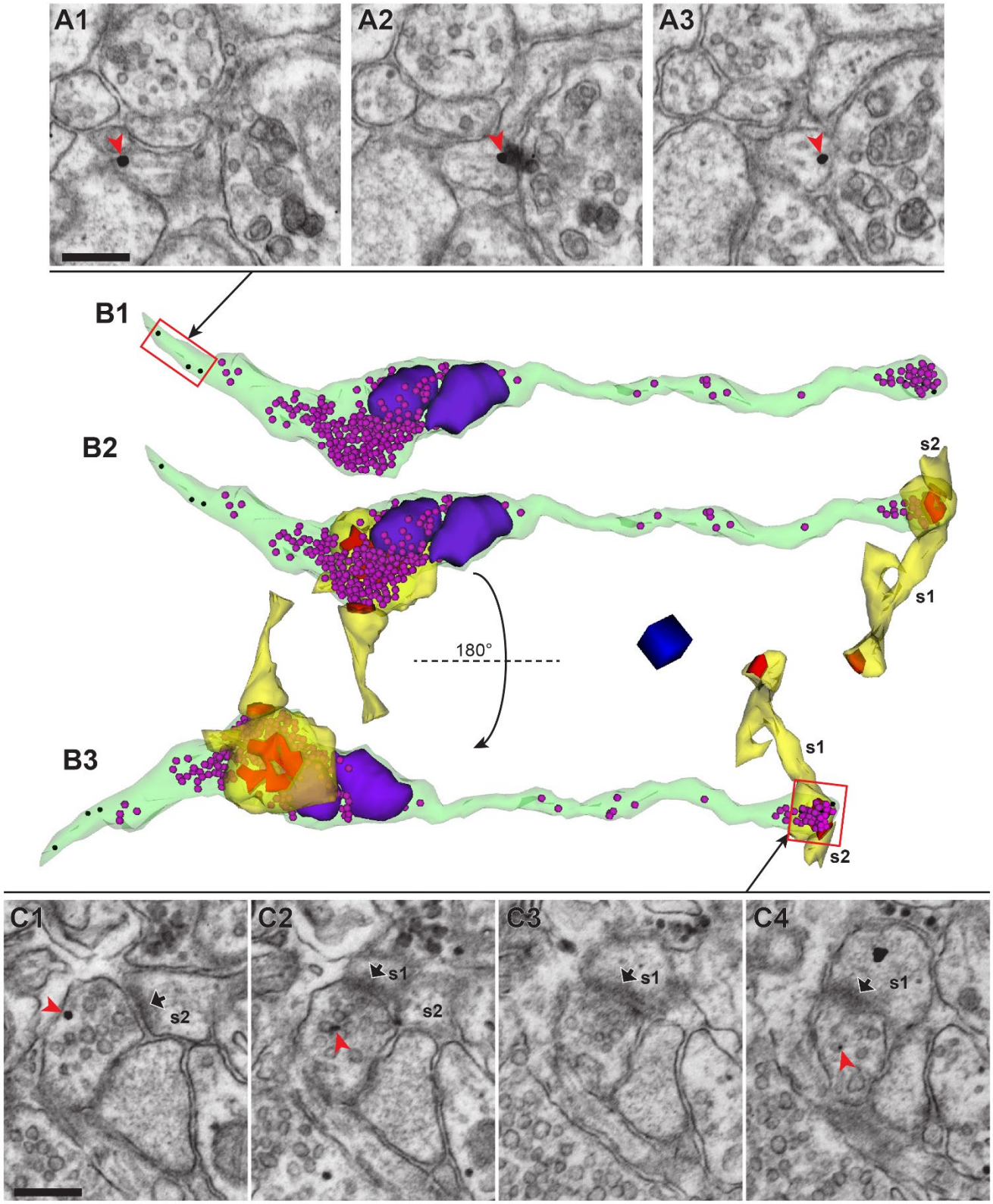

448

449 **Fig 4. Post-embedding immunogold labeling for Alexa Fluor dyes deposited by mAPEX2-driven TSA**

450 **reaction allowed for 3DEM identification of rAAV-targeted axons, while maintaining excellent**

451 **ultrastructure.** (**A1**-**A3**) Three adjacent serial tSEM images of an axon containing immunogold labeling (red

452 arrowhead). Scale bar = 250 nm. (**B1**) 3D reconstruction of the labeled axon (green) shown in **A**, which
453 contained immunogold labels (black spheres) and synaptic vesicles (magenta spheres). Two mitochondria
454 (purple) were associated with one of the two boutons. Red rectangle represents a portion of this axon shown in
455 **A1**-**A3**. (**B2**) Same axon as **B1**, with reconstructions of spines (yellow) forming synapses (red) with this axon.
456 Note, s1 was a branched spine with one of the heads forming a synapse with another axon. The second spine
457 (s2) and its PSD could be reconstructed only partially because they were located at the end of the tSEM image
458 series. Both axonal boutons are multi-synaptic, with each bouton forming synapses with two spines originating
459 from different dendrites. (**B3**) Same as **B2**, rotated along the horizontal axis 180° to provide a different view of
460 synapses and spines. One of the synapses at mitochondria-containing bouton was perforated (also see S1
461 Video). Red rectangle represents a portion of this axonal bouton shown in **C1**-**C4**. Scale cube = 250 nm per
462 side. (**C1**-**C4**) Four adjacent serial tSEM images of the gold-labeled (red arrowhead) axonal bouton, forming
463 synapses with two dendritic spines (s1 and s2; PSDs indicated by black arrows). Scale bar = 250 nm.
464

465 # Discussion

466 Genetic targeting of specific neuron populations for imaging and activation has transformed structure-
467 function studies of brain circuitry. Until now, however, tools for examining the ultrastructure of genetically
468 specified neurons post-manipulation have been lacking. Here we describe methods for inducing activity-
469 dependent plasticity in a genetically defined subset of neuronal synapses and for identifying optogenetically
470 potentiated axons. We demonstrate light-evoked L-LTP in acute hippocampal slices. Previous ultrastructural
471 studies of potentiated synapses examined effects across differentially activated populations of synapses, but
472 the histories of individual synapses were unknown. The unilateral infection of CA3 neurons yields CA3→CA1
473 projections that co-express a light-dependent actuator and an EM tag from a single rAAV amid a larger
474 population of unlabeled axons. Hence the advance of our approach is that recently potentiated synapses can
475 be compared to neighboring unstimulated synapses in the same block of tissue.
476

477 ## Light stimulation of CA3 axons resulted in robust oEPSP in ChR2-
478 ## expressing hippocampal slices

479 In hippocampal slices prepared from rAAV injected animals, light pulses induced oEPSP that depended
480 on voltage-gated sodium channels and GluA receptors. The light intensity used for optical high-frequency
481 stimulation (HFS) was shown to achieve the maximal responses. Furthermore, the expressed ChR2 reliably
482 responded to light trains delivered at 50 Hz, a frequency sufficient to produce L-LTP [10,43]. Together these
483 findings ensure that synapses identified by the *post hoc* 3DEM analysis were activated during the optogenetic
484 LTP induction protocol.
485

486 ## Optical L-LTP was produced in intact hippocampal slices expressing
487 ## ChR2-GFP and mAPEX2

488 We used high-frequency optical stimulation to induce GluN receptor-dependent L-LTP lasting at least 3
489 hr in a subpopulation of CA3→CA1 synapses containing presynaptically expressed ChR2. Recent reports
490 suggest molecular and synaptic asymmetry between right and left hippocampus affecting LTP induction and
491 endurance [11,46]. These findings prompted us to explore induction and expression of optical L-LTP in both
492 hemispheres. The rAAV was injected into the left (ipsilateral) or right (contralateral) hippocampus, and all slices
493 were prepared from the left hemisphere. L-LTP reached similar magnitudes whether the ipsilateral Schaffer
494 collaterals or contralateral commissural axons were optically stimulated.

495 This discrepancy with the prior papers could be due to technical differences, including recording
496 configurations (field vs. single-cell recordings) or plane of hippocampal slices (transverse vs. coronal). Our
497 findings are also consistent with prior studies using electrical stimulation. For example, in rat hippocampal
498 slices where Schaffer collaterals or commissural fibers were isolated by kainic acid lesion, the properties of
499 LTP produced independently by each pathway were similar to those observed in unlesioned slices [41,47].
500 Recent *in vivo* studies with intact brain also detected a robust LTP mediated by Schaffer or commissural axons
501 [48].
502

503 # Optical L-LTP did not require recruitment of unlabeled axons

504 In order to make direct comparisons between synapses with different activation histories, optical HFS
505 must activate only the rAAV-targeted axons. In the intact contralateral system, the measured oEPSP
506 responses could be contaminated if back-propagating action potentials from labeled commissural fibers were
507 to recruit neighboring unlabeled CA3 neurons through recurrent collaterals. To test whether our oEPSP
508 responses had been amplified through light-independent intra-hippocampal connections, we compared optical
509 stimulation in contralateral slices with intact or severed area CA3. Compared to intact slices, the cut slices had
510 a lower success rate for L-LTP (42% vs. 33%), yet these results suggest L-LTP could certainly be achieved
511 without recruitment of unlabeled axons.

512 There was a slower rise to maximum LTP magnitude in the cut slices that might have been caused by
513 reduced synchronicity of firing if unlabeled axons are recruited in the intact system. Other experiments have
514 witnessed this slow rise to LTP. For example, LTP can be produced with a slow onset with frequencies
515 normally used for induction of LTD (1-5 Hz) [49]. Sometimes weak presynaptic stimulation paired with
516 depolarization of postsynaptic neurons results in LTP with a similar slow rise early during expression [50,51].
517 Induction of mGluR-dependent [52] or BDNF-dependent LTP [53] both show slow rises in LTP magnitude.
518 Furthermore, at the developmental onset of L-LTP the expression can also have a slow rise [37]. Each of these
519 conditions is also submaximal in the induction paradigms, not unlike activation of less than all the axons with
520 light versus electrical stimulation. However, since both intact and cut slices expressed optically induced L-LTP
521 of the same magnitude at 2 and 3 hr post induction, the recruitment of unlabeled axons was unlikely to be the
522 critical factor.

523

524 # mAPEX2 labeled axons are compatible with ultrastructural analysis of
525 synapses

526 To study synaptic connectivity and function, it is necessary to know which synapses were engaged.
527 This level of analysis has been limited by the availability of ultrastructural tools to identify activated synapses.
528 We aimed to label the targeted axons discretely without obscuring or compromising the integrity of their

529 subcellular and synaptic components. Since the genetically encoded mAPEX2 was expressed in the tissue and
530 compatible with microwave-enhanced chemical fixation containing glutaraldehyde, it replaced the use of pre-
531 embedding antibody labeling to identify rAAV-targeted axons. mAPEX2 accommodates tyramide-conjugated
532 fluorescent dyes, which are then deposited in the targeted cells by the TSA reaction [54]. The combination of
533 mAPEX2-driven TSA reaction and post-embedding immunogold labeling allowed reliable identification of the
534 targeted cells throughout the 50 μm vibraslices, at depths not accessible by pre-embedding antibody methods
535 (< 10 μm). These features revealed optimal preservation of ultrastructure in acute slice tissue for analyses of
536 synapses and organelles after targeted optogenetic manipulations. We show that this process is compatible
537 with conventional fixation, processing, epoxy infiltration, and post-embedding immunogold labeling [55,56]. We
538 show that only a subset of serial sections need be labeled to track axons from the targeted cells, and even in
539 the labeled sections, the particles did not obscure objects of interest.

540 L-LTP induced by electrical theta-burst stimulation in the area CA1 is associated with an increase in the
541 abundance of multi-synaptic boutons in the population of stimulated axons [45]. The 3D reconstruction of a
542 labeled axon from an optogenetically potentiated slice showed two neighboring multi-synaptic boutons,
543 consistent with this prior report, but now from an identified axon. Future work will address whether such shifts
544 in synapse configurations are dependent on activation history.

545 The methods described here provide reliable physiology and labeling compatible with conventional
546 tissue fixation and the processing techniques needed to preserve subcellular organelles. They make an ideal
547 approach to link synapse ultrastructure and function in intact circuits of genetically defined neurons.
548

549 # Acknowledgements

550 The authors wish to thank the following colleagues for their help with this work: Stefanie Esmond and Bridget
551 Kajs for rAAV preparation; Geoff Dilly, Melissa Burks, Molly O'Gara for stereotaxic rAAV injections; John
552 Mendenhall for help with EM and useful discussions on labeling strategies; Dan Johnston for use of a Zeiss
553 light microscope and helpful discussions on electrophysiology; Nuno de Costa (Allen Institute for Brain
554 Science) for Ni-DAB protocol; Jung-Hwa Tao-Cheng (NINDS Electron Microscopy Facility) for suggesting the
555 use gold enhancement; Patrick Parker for help in preparing this manuscript. All are at the University of Texas
556 at Austin unless otherwise noted. The authors also acknowledge the following funding sources: Brain
557 Research Foundation Scientific Innovations Award (to K.M.H.), NSF Grant (1707356 to K.M.H.), NIH Grants
558 (MH095980, MH104319 and NS074644 to K.M.H.; EY026446, EY026442, and NS094330 to B.V.Z.), Human
559 Frontier Science Program (RGP0041 to B.V.Z.), and The University of Texas System UT BRAIN Seed Grants
560 (NNRI 365222 and 365289 to B.V.Z.).

561 # References

562 1. Bourne JN, Harris KM. Coordination of size and number of excitatory and inhibitory synapses results in a
563 balanced structural plasticity along mature hippocampal CA1 dendrites during LTP. Hippocampus.
564 2011;21: 354–373. doi:10.1002/hipo.20768

565 2. Ostroff LE, Fiala JC, Allwardt B, Harris KM. Polyribosomes Redistribute from Dendritic Shafts into Spines
566 with Enlarged Synapses during LTP in Developing Rat Hippocampal Slices. Neuron. 2002;35: 535–545.
567 doi:10.1016/S0896-6273(02)00785-7

568 3. Popov VI, Davies HA, Rogachevsky VV, Patrushev IV, Errington ML, Gabbott PLA, et al. Remodelling of
569 synaptic morphology but unchanged synaptic density during late phase long-term potentiation(ltp): A
570 serial section electron micrograph study in the dentate gyrus in the anaesthetised rat. Neuroscience.
571 2004;128: 251–262. doi:10.1016/j.neuroscience.2004.06.029

572 4. Smith HL, Bourne JN, Cao G, Chirillo MA, Ostroff LE, Watson DJ, et al. Mitochondrial support of
573 persistent presynaptic vesicle mobilization with age-dependent synaptic growth after LTP. eLife. 2016;5:
574 e15275. doi:10.7554/eLife.15275

575 5. Martell JD, Deerinck TJ, Sancak Y, Poulos TL, Mootha VK, Sosinsky GE, et al. Engineered ascorbate
576 peroxidase as a genetically encoded reporter for electron microscopy. Nat Biotechnol. 2012;30: 1143–
577 1148. doi:10.1038/nbt.2375

578 6. Lam SS, Martell JD, Kamer KJ, Deerinck TJ, Ellisman MH, Mootha VK, et al. Directed evolution of APEX2
579 for electron microscopy and proximity labeling. Nat Methods. 2015;12: 51–54. doi:10.1038/nmeth.3179

580 7. Nabavi S, Fox R, Proulx CD, Lin JY, Tsien RY, Malinow R. Engineering a memory with LTD and LTP.
581 Nature. 2014;511: 348–352. doi:10.1038/nature13294

582 8. Oishi N, Nomoto M, Ohkawa N, Saitoh Y, Sano Y, Tsujimura S, et al. Artificial association of memory
583 events by optogenetic stimulation of hippocampal CA3 cell ensembles. Mol Brain. 2019;12: 2.
584 doi:10.1186/s13041-018-0424-1

585 9. Chun S, Bayazitov IT, Blundon JA, Zakharenko SS. Thalamocortical Long-Term Potentiation Becomes
586 Gated after the Early Critical Period in the Auditory Cortex. J Neurosci. 2013;33: 7345–7357.
587 doi:10.1523/JNEUROSCI.4500-12.2013

588 10. Hashimotodani Y, Nasrallah K, Jensen KR, Chávez AE, Carrera D, Castillo PE. LTP at Hilar Mossy Cell-
589 Dentate Granule Cell Synapses Modulates Dentate Gyrus Output by Increasing Excitation/Inhibition
590 Balance. Neuron. 2017;95: 928-943.e3. doi:10.1016/j.neuron.2017.07.028

591 11. Kohl MM, Shipton OA, Deacon RM, Rawlins JNP, Deisseroth K, Paulsen O. Hemisphere-specific
592 optogenetic stimulation reveals left-right asymmetry of hippocampal plasticity. Nat Neurosci. 2011;14:
593 1413–1415. doi:10.1038/nn.2915

594 12. Zhang Y-P, Oertner TG. Optical induction of synaptic plasticity using a light-sensitive channel. Nat
595 Methods. 2007;4: 139–141. doi:10.1038/nmeth988

596 13. O'Riordan KJ, Hu N-W, Rowan MJ. Aß Facilitates LTD at Schaffer Collateral Synapses Preferentially in
597 the Left Hippocampus. Cell Rep. 2018;22: 2053–2065. doi:10.1016/j.celrep.2018.01.085

598 14. Berndt A, Schoenenberger P, Mattis J, Tye KM, Deisseroth K, Hegemann P, et al. High-efficiency
599 channelrhodopsins for fast neuronal stimulation at low light levels. Proc Natl Acad Sci. 2011;108: 7595–
600 7600. doi:10.1073/pnas.1017210108

601 15. Pédelacq J-D, Cabantous S, Tran T, Terwilliger TC, Waldo GS. Engineering and characterization of a
602 superfolder green fluorescent protein. Nat Biotechnol. 2006;24: 79–88. doi:10.1038/nbt1172

603 16. Stockklausner C, Ludwig J, Ruppersberg JP, Klöcker N. A sequence motif responsible for ER export and
604 surface expression of Kir2.0 inward rectifier K+ channels. FEBS Lett. 2001;493: 129–133.
605 doi:10.1016/S0014-5793(01)02286-4

606 17. Mittler R, Zilinskas BA. Molecular cloning and nucleotide sequence analysis of a cDNA encoding pea
607 cytosolic ascorbate peroxidase. FEBS Lett. 1991;289: 257–259. doi:10.1016/0014-5793(91)81083-K

608 18. Moriyoshi K, Richards LJ, Akazawa C, O'Leary DDM, Nakanishi S. Labeling Neural Cells Using
609 Adenoviral Gene Transfer of Membrane-Targeted GFP. Neuron. 1996;16: 255–260. doi:10.1016/S0896-
610 6273(00)80044-6

611 19. Kim JH, Lee S-R, Li L-H, Park H-J, Park J-H, Lee KY, et al. High Cleavage Efficiency of a 2A Peptide
612 Derived from Porcine Teschovirus-1 in Human Cell Lines, Zebrafish and Mice. PLOS ONE. 2011;6:
613 e18556. doi:10.1371/journal.pone.0018556

614 20. Borghuis BG, Tian L, Xu Y, Nikonov SS, Vardi N, Zemelman BV, et al. Imaging Light Responses of
615 Targeted Neuron Populations in the Rodent Retina. J Neurosci. 2011;31: 2855–2867.
616 doi:10.1523/JNEUROSCI.6064-10.2011

617 21. Grieger JC, Choi VW, Samulski RJ. Production and characterization of adeno-associated viral vectors.
618 Nat Protoc. 2006;1: 1412–1428. doi:10.1038/nprot.2006.207

619 22. Aurnhammer C, Haase M, Muether N, Hausl M, Rauschhuber C, Huber I, et al. Universal Real-Time PCR
620 for the Detection and Quantification of Adeno-Associated Virus Serotype 2-Derived Inverted Terminal
621 Repeat Sequences. Hum Gene Ther Methods. 2012;23: 18–28. doi:10.1089/hgtb.2011.034

622 23. Yuste R, Miller RB, Holthoff K, Zhang S, Miesenbo¨ck G. Synapto-pHluorins: Chimeras between pH-
623 sensitive mutants of green fluorescent protein and synaptic vesicle membrane proteins as reporters of
624 neurotransmitter release. In: Thorner J, Emr SD, Abelson JN, editors. Methods in Enzymology. Academic
625 Press; 2000. pp. 522–546. doi:10.1016/S0076-6879(00)27300-X

626 24. Bourne JN, Kirov SA, Sorra KE, Harris KM. Warmer preparation of hippocampal slices prevents synapse
627 proliferation that might obscure LTP-related structural plasticity. Neuropharmacology. 2007;52: 55–59.
628 doi:10.1016/j.neuropharm.2006.06.020

629 25. Bourne JN, Harris KM. Nanoscale analysis of structural synaptic plasticity. Curr Opin Neurobiol. 2012;22:
630 372–382. doi:10.1016/j.conb.2011.10.019

631 26. Harris KM, Teyler TJ. Developmental onset of long-term potentiation in area CA1 of the rat hippocampus.
632 J Physiol. 1984;346: 27–48. doi:10.1113/jphysiol.1984.sp015005

633 27. Jensen FE, Harris KM. Preservation of neuronal ultrastructure in hippocampal slices using rapid
634 microwave-enhanced fixation. J Neurosci Methods. 1989;29: 217–230. doi:10.1016/0165-0270(89)90146-
635 5

636 28. Harris KM, Perry E, Bourne J, Feinberg M, Ostroff L, Hurlburt J. Uniform Serial Sectioning for
637 Transmission Electron Microscopy. J Neurosci. 2006;26: 12101–12103. doi:10.1523/JNEUROSCI.3994-
638 06.2006

639 29. Kuwajima M, Mendenhall JM, Harris KM. Large-Volume Reconstruction of Brain Tissue from High-
640 Resolution Serial Section Images Acquired by SEM-Based Scanning Transmission Electron Microscopy.
641 In: Sousa AA, Kruhlak MJ, editors. Nanoimaging. Humana Press; 2013. pp. 253–273. doi:10.1007/978-1-
642 62703-137-0_15

643 30. Reynolds ES. The use of lead citrate at high pH as an electron-opaque stain in electron microscopy. J
644 Cell Biol. 1963;17: 208–212.

645 31. Kuwajima M, Mendenhall JM, Lindsey LF, Harris KM. Automated Transmission-Mode Scanning Electron
646 Microscopy (tSEM) for Large Volume Analysis at Nanoscale Resolution. PLoS ONE. 2013;8: e59573.
647 doi:10.1371/journal.pone.0059573

648 32. Schindelin J, Arganda-Carreras I, Frise E, Kaynig V, Longair M, Pietzsch T, et al. Fiji: an open-source
649 platform for biological-image analysis. Nat Methods. 2012;9: 676–682. doi:10.1038/nmeth.2019

650 33. Cardona A, Saalfeld S, Schindelin J, Arganda-Carreras I, Preibisch S, Longair M, et al. TrakEM2
651 Software for Neural Circuit Reconstruction. PLoS ONE. 2012;7: e38011.
652 doi:10.1371/journal.pone.0038011

653 34. Saalfeld S, Fetter R, Cardona A, Tomancak P. Elastic volume reconstruction from series of ultra-thin
654 microscopy sections. Nat Methods. 2012;9: 717–720. doi:10.1038/nmeth.2072

655 35. Fiala JC. Reconstruct: a free editor for serial section microscopy. J Microsc. 2005;218: 52–61.
656 doi:10.1111/j.1365-2818.2005.01466.x

657 36. Fiala JC, Harris KM. Cylindrical diameters method for calibrating section thickness in serial electron
658 microscopy. J Microsc. 2001;202: 468–472. doi:10.1046/j.1365-2818.2001.00926.x

659 37. Cao G, Harris KM. Developmental regulation of the late phase of long-term potentiation (L-LTP) and
660 metaplasticity in hippocampal area CA1 of the rat. J Neurophysiol. 2012;107: 902–912.
661 doi:10.1152/jn.00780.2011

662 38. Isomura Y, Fujiwara-Tsukamoto Y, Imanishi M, Nambu A, Takada M. Distance-Dependent Ni2+-
663 Sensitivity of Synaptic Plasticity in Apical Dendrites of Hippocampal CA1 Pyramidal Cells. J Neurophysiol.
664 2002;87: 1169–1174. doi:10.1152/jn.00536.2001

665 39. Kloosterman F, Peloquin P, Leung LS. Apical and Basal Orthodromic Population Spikes in Hippocampal
666 CA1 In Vivo Show Different Origins and Patterns of Propagation. J Neurophysiol. 2001;86: 2435–2444.
667 doi:10.1152/jn.2001.86.5.2435

668 40. Leung LW. Potentials evoked by alvear tract in hippocampal CA1 region of rats. I. Topographical
669 projection, component analysis, and correlation with unit activities. J Neurophysiol. 1979;42: 1557–1570.
670 doi:10.1152/jn.1979.42.6.1557

671 41. Wheal HV, Lancaster B, Bliss TVP. Long-term potentiation in Schaffer collateral and commissural
672 systems of the hippocampus: In vitro study in rats pretreated with kainic acid. Brain Res. 1983;272: 247–
673 253. doi:10.1016/0006-8993(83)90570-X

674 42. Jackman SL, Beneduce BM, Drew IR, Regehr WG. Achieving High-Frequency Optical Control of Synaptic
675 Transmission. J Neurosci. 2014;34: 7704–7714. doi:10.1523/JNEUROSCI.4694-13.2014

676 43. Zakharenko SS, Zablow L, Siegelbaum SA. Visualization of changes in presynaptic function during long-
677 term synaptic plasticity. Nat Neurosci. 2001;4: 711. doi:10.1038/89498

678 44. Hainfeld JF, Powell RD. New Frontiers in Gold Labeling. J Histochem Cytochem. 2000;48: 471–480.
679 doi:10.1177/002215540004800404

680 45. Bourne JN, Chirillo MA, Harris KM. Presynaptic Ultrastructural Plasticity Along CA3→CA1 Axons During
681 Long-Term Potentiation in Mature Hippocampus. J Comp Neurol. 2013;521: 3898–3912.
682 doi:10.1002/cne.23384

683 46. Shinohara Y, Hirase H, Watanabe M, Itakura M, Takahashi M, Shigemoto R. Left-right asymmetry of the
684 hippocampal synapses with differential subunit allocation of glutamate receptors. Proc Natl Acad Sci.
685 2008;105: 19498–19503. doi:10.1073/pnas.0807461105

686 47. Bliss TV, Lancaster B, Wheal HV. Long-term potentiation in commissural and Schaffer projections to
687 hippocampal CA1 cells: an in vivo study in the rat. J Physiol. 1983;341: 617–626.
688 doi:10.1113/jphysiol.1983.sp014828

689 48. Martin SJ, Shires KL, da Silva BM. Hippocampal Lateralization and Synaptic Plasticity in the Intact Rat:
690 No Left–Right Asymmetry in Electrically Induced CA3-CA1 Long-Term Potentiation. Neuroscience.
691 2019;397: 147–158. doi:10.1016/j.neuroscience.2018.11.044

692 49. Habib D, Dringenberg HC. Low-frequency-induced synaptic potentiation: A paradigm shift in the field of
693 memory-related plasticity mechanisms? Hippocampus. 2010;20: 29–35. doi:10.1002/hipo.20611

694 50. Magee JC, Johnston D. A Synaptically Controlled, Associative Signal for Hebbian Plasticity in
695 Hippocampal Neurons. Science. 1997;275: 209–213. doi:10.1126/science.275.5297.209

696 51. Markram H, Lübke J, Frotscher M, Sakmann B. Regulation of Synaptic Efficacy by Coincidence of
697 Postsynaptic APs and EPSPs. Science. 1997;275: 213–215. doi:10.1126/science.275.5297.213

698 52. Bortolotto ZA, Collingridge GL. Characterisation of LTP induced by the activation of glutamate
699 metabotropic receptors in area CA1 of the hippocampus. Neuropharmacology. 1993;32: 1–9.
700 doi:10.1016/0028-3908(93)90123-K

701 53. Kang H, Schuman EM. Long-lasting neurotrophin-induced enhancement of synaptic transmission in the
702 adult hippocampus. Science. 1995;267: 1658–1662. doi:10.1126/science.7886457

703 54. Lee J, Song EK, Bae Y, Min J, Rhee H-W, Park TJ, et al. An enhanced ascorbate peroxidase 2/antibody-
704 binding domain fusion protein (APEX2–ABD) as a recombinant target-specific signal amplifier. Chem
705 Commun. 2015;51: 10945–10948. doi:10.1039/C5CC02409A

706 55. Coleman RA, Liu J, Wade JB. Use of anti-fluorophore antibody to achieve high-sensitivity
707 immunolocalizations of transporters and ion channels. J Histochem Cytochem Off J Histochem Soc.
708 2006;54: 817–827. doi:10.1369/jhc.6A6929.2006

709 56. Oberti D, Kirschmann MA, Hahnloser RHR. Correlative microscopy of densely labeled projection neurons
710 using neural tracers. Front Neuroanat. 2010;4: 24. doi:10.3389/fnana.2010.00024

711 57. Paxinos G, Franklin KBJ. The Mouse Brain in Stereotaxic Coordinates. 2nd edition. San Diego: Academic
712 Press; 2001.

713

Supporting information

S1 Fig. Verification of rAAV injections and further characterization of oEPSP at CA3→CA1 synapses. (**A**-**B**) Unilateral injections of rAAV into the area CA3 result in GFP labeling of Schaffer collaterals and commissural fibers. (**A**) A diagram (modified from ref. [57]) showing the approximate site of rAAV injection site in the mouse hippocampal area CA3. An infected CA3 neuron (green) on the right hemisphere depicted under the injection needle (magenta) projects its axons to synapse onto neurons in both ipsilateral and contralateral CA1 via Schaffer collaterals and commissural fibers, respectively. These axons can also synapse onto uninfected CA3 neurons (black). (**B**) A montage of two epifluorescence images of a coronal section through the injection site in the right area CA3. The right hemisphere (injected side) was partially damaged during extraction of the brain. Scale bar = 1 mm. (**C**-**F**) In acute transverse slices of the hippocampus prepared from rAAV injected mice, light pulse stimulation of the virally targeted CA3 axons evoked oEPSPs in the area CA1. (**C**) Example traces of oEPSPs recorded from an electrode positioned in different CA1 layers (colored circles): strata oriens (SO), pyramidale (SP), radiatum (SR), and lacunosum-moleculare (SLM). Optical fiber was placed in SR in the proximal area CA1, ~400 μm from the recording electrode. Scale bars = 5 ms, 1 mV. (**D**) Amplitude (left) and slope (right) of optically and electrically evoked field EPSPs. Optical stimulation was delivered at the maximum light intensity, while electrical stimulation was at half-maximum. Horizontal lines and error bars indicate mean ± SEM. The number of slices used for each condition is indicated in parentheses. (**E**) Optical paired-pulse stimulation induces slight facilitation (mean ± SEM, n = 6 slices). Scale bars = 10 ms, 1 mV. (**F**) oEPSP was blocked by application of 1 μM TTX (left) or by 20 μM DNQX (right). Scale bars = 5 ms, 1 mV (TTX); 5 ms, 2 mV (NBQX). The recordings shown in **D**-**F** were made from the middle SR.

S2 Fig. Input-output (IO) curves recorded from the area CA1 in intact and cut slices. (**A**) Representative oEPSP traces recorded from a slice with intact CA3. (**B**) Same as **A**, but recorded from a cut slice. Scale bars = 1 ms, 1 mV for **A** and **B**. (**C**) Optical IO curves recorded from intact and cut slices. The intensities of light stimulation used to record optical IO: 30% (~4 mW), 60% (~9mW), 90% (~13mW), and 100% (~14.5 mW). There is no significant difference between responses evoked by 90% and 100% light intensities ($t = 0.317$, $df = 10$, $p > 0.05$ for intact slices; $t = 0.342$, $df = 9$, $p > 0.05$ for cut slices; two-sided paired t-test). (**D**) Summary of

741 oEPSP slope (left) and amplitude (right) recorded at the maximum light power. (**E**) Input-output curves
742 recorded using an electrical stimulation. (**F**) Summary of eEPSP slope (left) and amplitude (right) recorded at
743 intensity that resulted in approximately half-maximum slope. All graphs (**C**-**F**) show mean ± SEM. Different sets
744 of slices were analyzed for **C** and **D**; **E** and **F**. The number of slices used for each condition is indicated in
745 parentheses.
746
747 **S3 Fig. Enzymatic activity of mAPEX is preserved after chemical fixation with glutaraldehyde.**
748 Diaminobenzidine (DAB) was used as a substrate because autofluorescence from glutaraldehyde makes it
749 difficult to assess labeling with tyramide-conjugated fluorescent dyes. (**A**) Right: mAPEX1 expressed in
750 dissociated rat hippocampal neurons, fixed with 6% glutaraldehyde and 2% formaldehyde, were capable of
751 generating the dark brown DAB reaction product. Left: Control neurons fixed and treated with DAB in the same
752 manner did not exhibit the reaction product. Scale bars = 50 μm. (**B**) Two serial tSEM images showing axons
753 labeled with Ni-enhanced DAB (red contours) through the area CA1 from a perfusion-fixed C57B/6J mouse.
754 The rAAV was injected into the ipsilateral hippocampal area CA1 to express mAPEX2. The fixative contained
755 2.5% glutaraldehyde and 2% formaldehyde. Scale bars = 500 nm. Insets: Enlarged areas indicated by black
756 rectangles. Electron-dense Ni-DAB reaction product obscures subcellular structures in the labeled axons. In
757 contrast, small synaptic vesicles are visible in an unlabeled axonal bouton nearby (ax). Scale bars = 100 nm.
758
759 **S4 Fig. Electron-dense artifacts and subcellular structures present in unlabeled sections.** Electron-
760 dense artifacts and subcellular structures present in unlabeled sections. Five serial tSEM images from the
761 series presented in Fig 3C. These images were acquired from serial thin sections that were not immunolabeled
762 for Alexa Fluor dye, but stained with uranyl acetate and lead citrate (UA/Pb) prior to tSEM imaging. While
763 glycogen granules fill glial processes (green arrowheads in 'g'), they are less common in axons (ax) and
764 boutons (b1, b2, and b3) and do not appear in the same profiles over two consecutive sections (yellow
765 arrowheads). Post-section staining with UA/Pb can be a source of electron-dense artifacts of various size and
766 shape (purple arrowheads) that are usually confined to single sections. On rare occasions, small artifacts could
767 appear in two consecutive sections. However, their small size (diameter ≤ 10 nm) is similar to those generated

768 as a result of background nucleation during gold enhancement (see S5 Fig), and therefore, can easily be
769 distinguished from positive labeling should they also occur in immunolabeled sections. Scale bar = 250 nm.
770
771 **S5 Fig. Electron-dense artifacts due to gold enhancement reagent. Electron-dense artifacts due to gold**
772 **enhancement reagent.** (**A**) A histogram showing the distribution of diameters of gold-enhanced gold particles
773 (bin size = 2 nm). A total of 527 particles were analyzed with Fiji software (see Online Methods). Their
774 diameter ranged from 2.5 nm to 85.3 nm with the median of 37.1 nm and the mean of 36.5 ± 0.61 nm (SEM). A
775 vertical line at 10 nm indicates the cutoff for gold particles excluded during identification of labeled axons. (**B**) A
776 tSEM image acquired from serial thin sections that were not immunolabeled, but incubated with the gold
777 enhancement reagent and then stained with uranyl acetate and lead citrate. Small electron-dense particles
778 (indicated by dotted red circles) were 10 nm or smaller in diameter, and were present in dendrites (den), axons
779 (ax), and boutons (b). These small particles likely formed as a result of self-nucleation of gold enhancement
780 reagent, and therefore were excluded during identification of labeled axons. Scale bar = 250 nm.
781
782 **S1 Video. A video of the reconstructed axon shown in Fig 4.** File name: S1_video.mp4. File size: 71.1 MB.
783 This video is also available as an external file – see Data Availability.

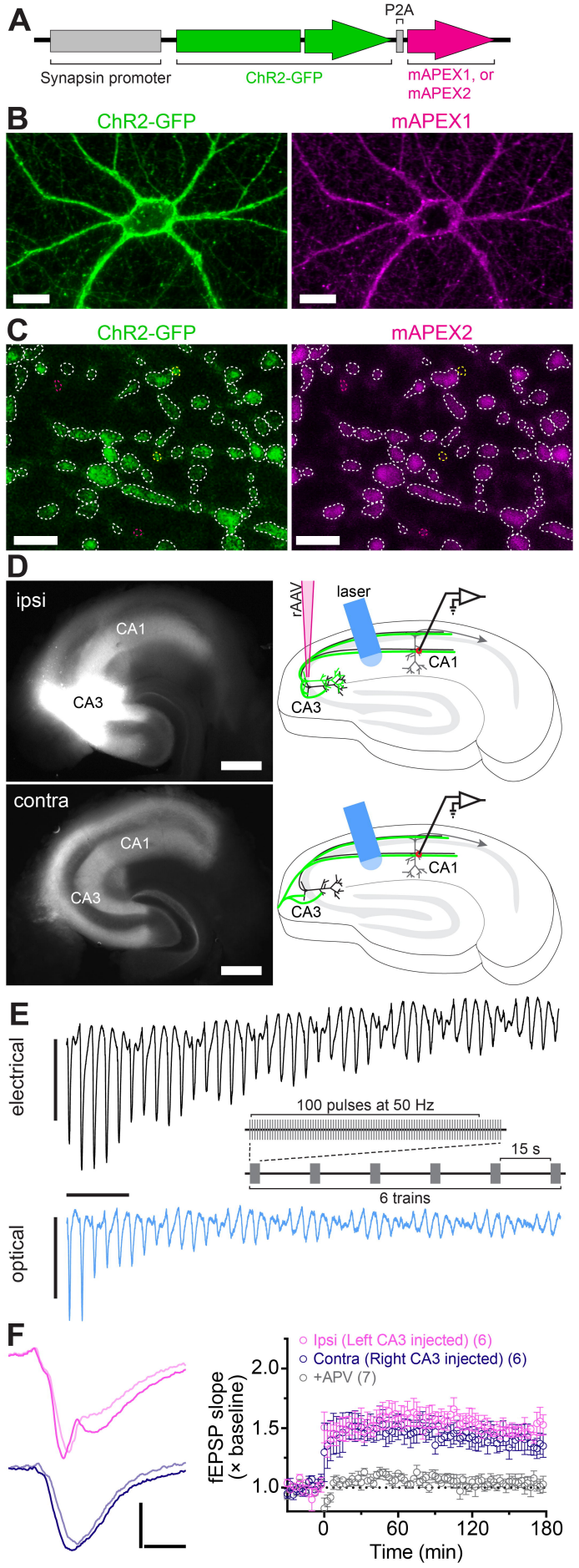
A
P2A
Synapsin promoter
ChR2-GFP
mAPEX1, or
mAPEX2
B
ChR2-GFP
mAPEX1
C
ChR2-GFP
mAPEX2
D
ipsi
CA1
CA3
contra
CA1
CA3
rAAV
laser
CA1
CA3
CA1
CA3
E
electrical
100 pulses at 50 Hz
15 s
6 trains
optical
F
Ipsi (Left CA3 injected) (6)
Contra (Right CA3 injected) (6)
+APV (7)
fEPSP slope
(× baseline)
2.0
1.5
1.0
0
60
120
180
Time (min)

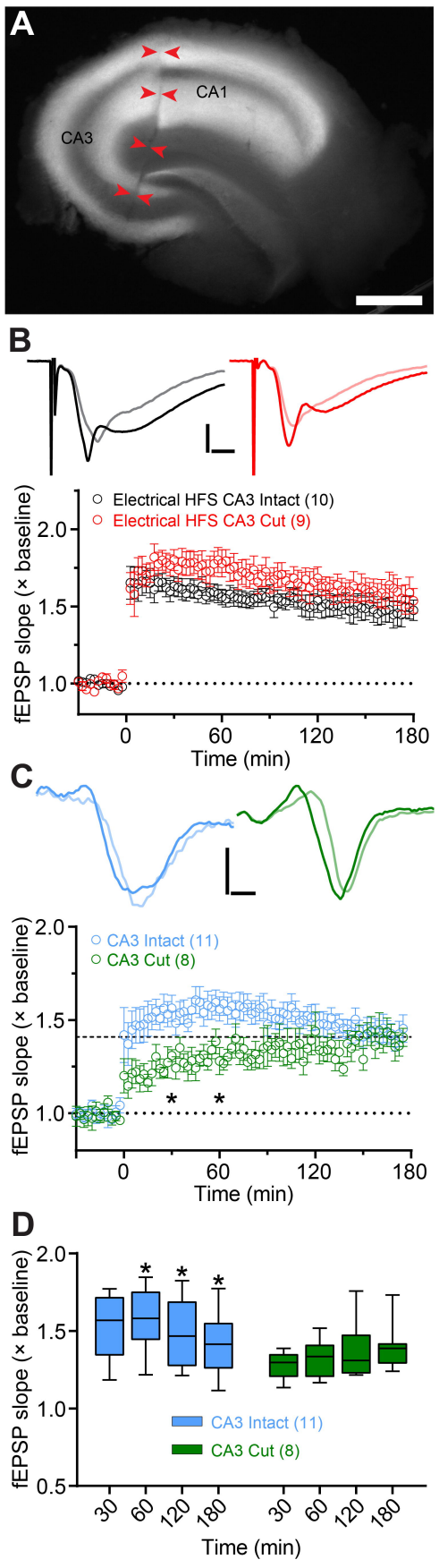
A
CA1
CA3
B
Electrical HFS CA3 Intact (10)
Electrical HFS CA3 Cut (9)
fEPSP slope (× baseline)
2.0
1.5
1.0
0
60
120
180
Time (min)
C
CA3 Intact (11)
CA3 Cut (8)
fEPSP slope (× baseline)
2.0
1.5
1.0
*
*
0
60
120
180
Time (min)
D
fEPSP slope (× baseline)
2.0
1.5
1.0
0.5
*
*
*
CA3 Intact (11)
CA3 Cut (8)
30
60
120
180
30
60
120
180
Time (min)

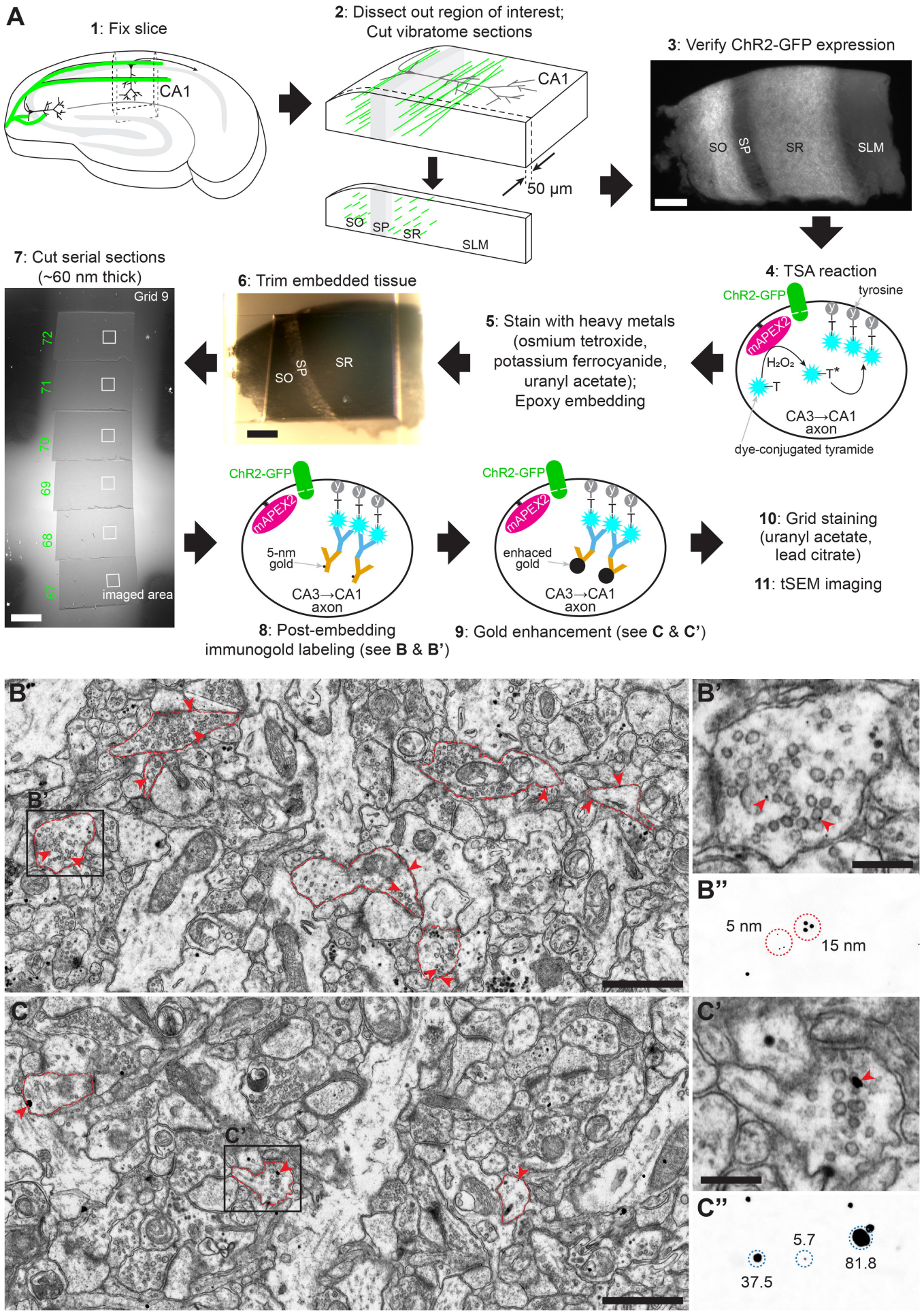
A
1: Fix slice
CA1
2: Dissect out region of interest;
Cut vibratome sections
CA1
50 µm
SO
SP
SR
SLM
3: Verify ChR2-GFP expression
SO
SP
SR
SLM
4: TSA reaction
ChR2-GFP
tyrosine
mAPEX2
H₂O₂
T
T*
CA3→CA1
axon
dye-conjugated tyramide
5: Stain with heavy metals
(osmium tetroxide,
potassium ferrocyanide,
uranyl acetate);
Epoxy embedding
6: Trim embedded tissue
SO
SP
SR
7: Cut serial sections
(~60 nm thick)
Grid 9
72
71
70
69
68
67
imaged area
ChR2-GFP
mAPEX2
5-nm
gold
CA3→CA1
axon
8: Post-embedding
immunogold labeling (see B & B')
ChR2-GFP
mAPEX2
enhaced
gold
CA3→CA1
axon
9: Gold enhancement (see C & C')
10: Grid staining
(uranyl acetate,
lead citrate)
11: tSEM imaging
B
B'
B'
B''
5 nm
15 nm
C
C'
C'
C''
5.7
37.5
81.8

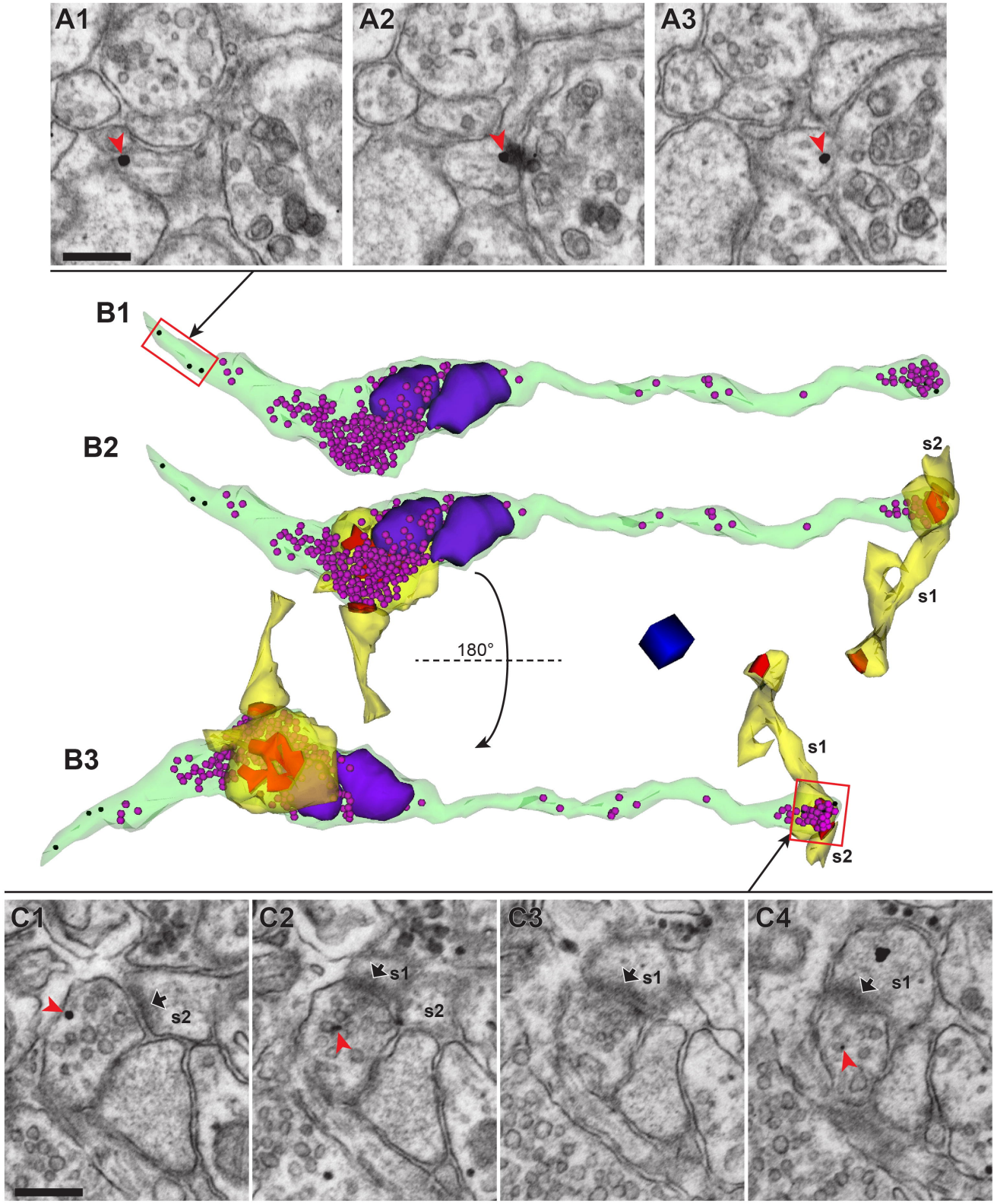
A1
A2
A3
B1
B2
B3
s2
s1
180°
s1
s2
C1
s2
C2
s1
s2
C3
s1
C4
s1